Design Strategy of Conventional Electronic for Wireless Sensor Node Powered by Vibration Energy Harvester

Florian Huet, Vincent Boitier

International Conference on Renewable Energies and Power Quality (ICREPQ'19)
Tenerife (Spain), 10th to 12th April, 2019
Renewable Energy and Power Quality Journal (RE&PQJ)
ISSN 2172-038 X, No.17 April 2019

Design Strategy of Conventional Electronic for Wireless Sensor Node Powered by Vibration Energy Harvester

F. Huet and V. Boitier

[1] LAAS-CNRS, Université de Toulouse, CNRS, UPS
7 Avenue du colonel Roche
F-31400 Toulouse (France)
Phone: +33 561 33 62 31, e-mail: florian.huet@laas.fr, vincent.boitier@laas.fr

Abstract. This article presents the design strategy for the power management electronics of a wireless sensor node (WSN) powered by vibration energy harvesting. The energy harvester employed is a commercial piezoelectric cantilever. The electronic structure proposed is composed of LTC3588-1 extraction circuit, super-capacitors storage with balancing sub-system and activation switch output sub-system. To validate this architecture, a prototype has been developed and experimental results are presented.

Key words: Piezoelectric generator, Vibration energy harvesting, Energy management, AC/DC converter.

1. Introduction

The deployment of IoT (Internet of Things) in the industrial, transport and health sectors is emerging. The knowledge of information at any point in a system becomes a necessity to improve its control. The integration of wireless sensors node (WSN) is one of the solutions considered. Today, few systems are currently deployed. However, companies like Libelium [1] offer a vision of a smart city, where their sensors can be deployed to collect several environmental data. WSN can be used in public infrastructure monitoring, such as the Los Angeles Golden Gate [2], where the integrity of the structure over time is monitored by vibration sensors. Researchers are using WSNs to understand the behavior of seabirds nesting on Great Duck Island by collecting physical data from the site (temperature, moisture or pressure) [3]. But still, the monitoring of the Tungurahua volcano is made with WSN carrying seismographs [4]. However, the energy autonomy of the latter hinders their deployment [5], [6]. Many solutions exploiting the ambient energy harvesting are being developed. The nature of the energy harvested depends on the environment of the place to be instrumented. It is possible to recover thermal, solar, vibratory energy and many others [7]. The use of piezoelectric generators for energy harvesting is highly studied and simple to implement [8]. The extraction circuits are also strongly studied in order to improve the performances [7]. Nevertheless, these systems are not industrialized and marketed. In the context of industrial projects, it may be essential to integrate from the design stage the use of available and reliable commercial circuits. For piezoelectric device, the commercial circuit LTC3588-1 [9] is commonly used, but architecture are rarely optimized [10]–[13]. In this article, we also propose a design strategy of an energy management circuit based on commercial circuit to supply a WSN powered by vibratory energy harvesting. Our solution offers versatility to manage the different phases of consumption of a WSN and to handle variability or discontinuity of the vibration source.

2. Architecture

The overall architecture of the complete WSN system adapted for vibratory energy harvesting is shown in Fig. 1.

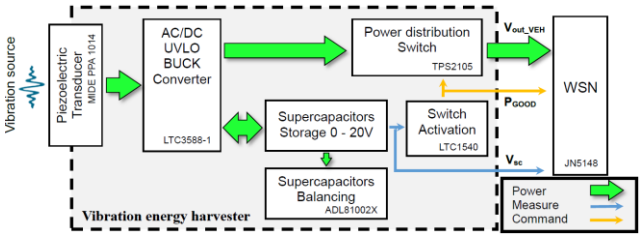

Fig. 1. Electromechanical architecture of device

The presented structure is composed by a piezoelectric transducer as cantilever beam type, an extraction circuit having the role of AC / DC converter, a storage composed of super-capacitors and its balancing system. A sub-system composed of a power distribution switch and a hysteresis comparator makes it possible to select the thresholds for activating or not the output. The WSN can then be powered (V_{out_VEH}) and receive different information such as super-capacitance voltage (V_{sc}) or a fraction of this voltage and information on the state of activation of the output voltage (P_{GOOD}). This latter information is useful in the event of the WSN has a second power source. This architecture avoids oversizing the energy storage and uses better the capacitors energy while reducing the electronic overall volume.

3. Power producer and consumer

A. Piezoelectric vibration energy harvester (VEH)

Mechanical energy from a vibration source is converted into electrical energy using a piezoelectric transducer. In this paper, we use a simple cantilever beam MIDE PPA 1014 [14] as a linear inertial generator (Fig. 2).

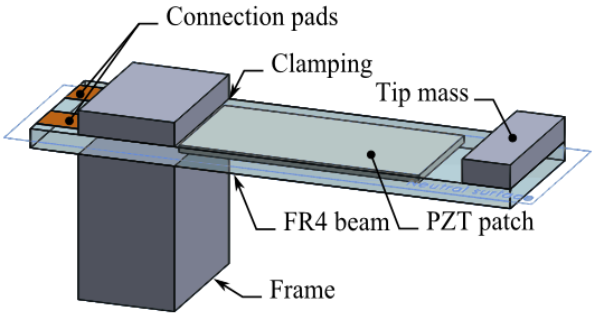

Fig. 2. Piezoelectric VEH architecture

Its sizing was selected to obtain a first mode resonance frequency corresponding to the excitation frequency of the source, so a frequency of 128.8 Hz and an acceleration of 14 m/s². The length of the beam is 26.5 mm and the total dynamic mass is 3.8 g. This device is solicited at a constant acceleration of 14 m/s² for the characterisation. To finely characterize the device used, a frequency sweep (100 Hz to 150 Hz) and a load resistance sweep (100 Ω to 800 kΩ) is performed in order to deduce the optimal performance of operation. This operation is obtained with the use of a test bench developed in previous work [15]. Fig. 3 represents the RMS voltage measured across the load resistance as a function of itself and the excitation frequency.

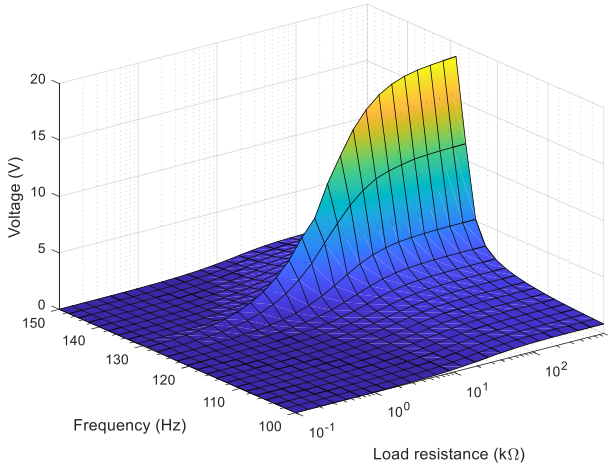

Fig. 3. VEH voltage output measurement

The maximum voltage reached at resonance is 18.81 V for the 800 kΩ load resistance. Fig. 4 represents the power dissipated in the load resistance according to the latter and the excitation frequency. The maximum power measured experimentally is 5.8 mW (if the beam is connected to a 27.5 kΩ load resistance). However, rectifying the signal affects the power by a factor π/2 [16] reducing it to 3.7 mW. It must be noticed that the power produced is very sensitive to frequency (the bandwidth is 5 Hz) and acceleration fluctuations of the source.

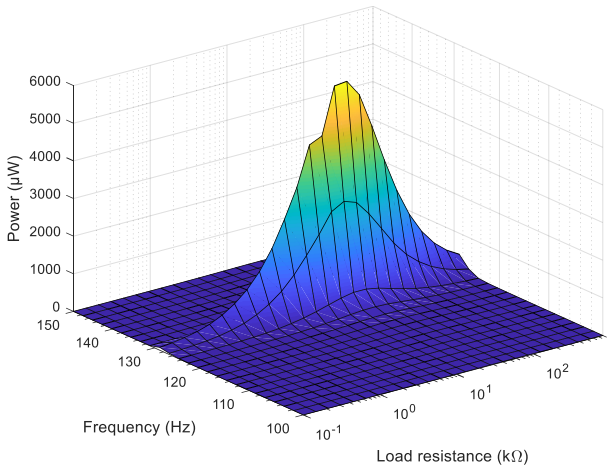

Fig. 4. VEH power output measurement

B. Wireless sensor node

The WSN to be powered is a JENNIC JN5148 module in "End Device" configuration (Fig. 5) capable of measuring and transmitting two temperatures and its own supply voltage. A second JENNIC module in “Coordinator” configuration ensures the radio connection. The supply voltage of these modules ranges from 2.8 V to 3.6 V, for tests we feed it at 3.3 V.

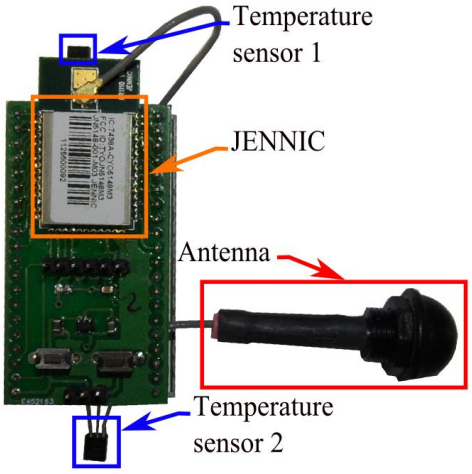

Fig. 5. JENNIC JN5148 “End Device” module

This WSN has three main operating phases: the initialisation phase, which include the cold-start, the connection to the network, and a 307 s transitive period of the module (helpful to verify the good reception of the signal). Then the WSN switches between the measurement & transmission phase and the sleep mode phase. The currents needed by the various operating phases of the JENNIC are shown in Fig. 6. The energy, duration, and maximum peak power of these phases are listed in Table 1.

Table 1. Operation phases characteristics

Phase	Energy	Duration	Peak power
Initialisation	389.4 mJ	311 s	180.8 mW
Meas. & trans.	3.2 mJ	110 ms	213.2 mW
Sleep	3.8 mJ	46.9 s	87.45 mW

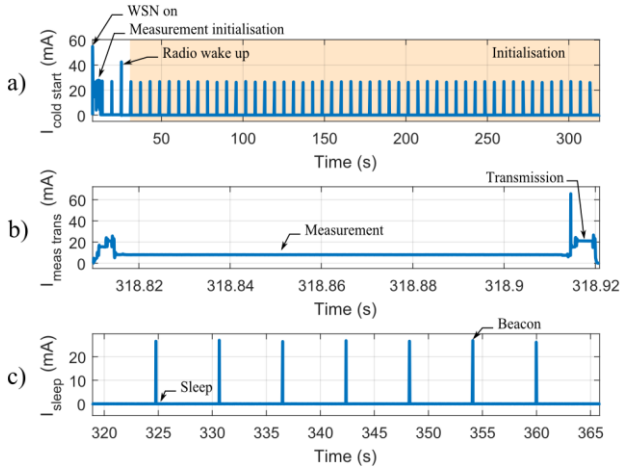

Fig. 6. JENNIC current consumptions of a) initialisation, b) measurement & transmission and c) sleep phases

Fig. 6a shows the consumption of the initialisation phase. It is composed of a start-up peak (54.8 mA), a plateau of initialisation of the measurement sensors, a peak of connection (42.5 mA) to the "coordinator" and a long period sprinkled with peaks initialisation (26.7 mA) of the system where a frame is sent every 5.8 s. The energy required to achieve this phase is 398.4 mJ over a total duration of 311 s. Following this phase, a first measurement and transmission of information begins (Fig. 6b). The sensors wake up and do the measurements. The radio wakes up (64.6 mA) and transmits the data. This phase requires 3.2 mJ and lasts 110 ms. The sleep mode phase (Fig. 6c) is scalable and sets the measurement rate. The observable peaks (26.5 mA) in Fig. 6c are transmitted frames to allow the "coordinator" to verify that the "end device" is still connected. In this case, a measurement in realized each 46.9 s and requires 3.8 mJ.

C. Confrontation between producer and consumer

The confrontation between the power produced by the harvester (<3.7 mW) and the WSN power required to do the measurement and the information transmission (29.1 mW) shows the need of a storage block in an efficient and timely manner. However, some phases can be theoretically powered directly. Multiple peaks require significant instantaneous power, such as the first peak (180.8 mW) or the transmission peak (213.18 mW). It is necessary to consider these events to properly start the WSN and avoid disconnection.

4. Electronic design strategy

A. Extraction circuit

The piezoelectric transducer used can provide high AC voltage levels (≈ 20 V), but the current is very low (< 150 µA). The alternating shape of the electrical energy produced is not exploitable as it is. A formatting is then necessary. For this, we use the LTC3588-1 [9] extraction circuit presented in Fig. 7. The circuit consists of a diode bridge to rectify the voltage from the transducer. The rectified voltage V_{in} is limited to 20 V by a Zener diode. A buck DC/DC converter follows the bridge and provides an output voltage level V_{OUT} adjustable using logical inputs D0 and D1. Four possibilities can be selected (1.8 V, 2.5 V, 3.3 V and 3.6 V). In our case, we choose an output voltage V_{OUT} of 3.3 V. The circuit requires capacitors C_1 and C_2, which provide a stock of energy necessary for the internal operation. The inductor L_1 provides modulation of the energy transfer frequency via the buck.

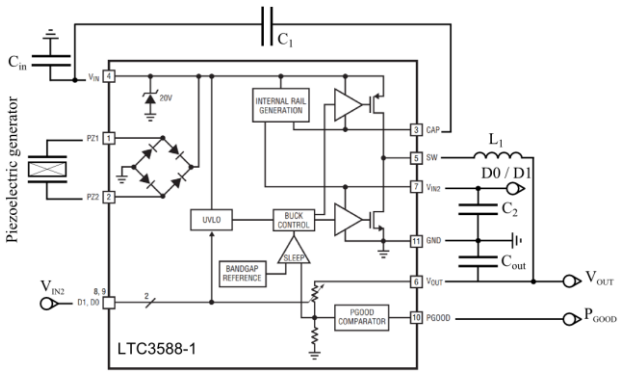

Fig. 7. LTC3588-1 block diagram

The assembly requires a capacitor (C_{in}) between V_{in} and Gnd and another capacitor (C_{out}) is necessary at the output between V_{out} and Gnd. The storage block is mainly located on C_{in} or on C_{out}. Depending on V_{in}, the energy transfer from C_{in} to C_{out} is managed by the output of a hysteresis comparator which allows or not the buck converter. It is connected if $V_{in} > 5.05$ V and disconnected if $V_{in} < 3.67$ V. It works as an UVLO (UnderVoltage Lock Out) circuit. Fig. 8 represents the regulation and transfer of the energy stored in C_{in} towards C_{out} over time. During these phases and despite a low incoming current, the efficiency of this circuit is greater than 80 % thanks to its simplicity. However, the power transfer is limited by a maximum current value of 100 mA. This value can be reduced according to the ESR of the super-capacitors used.

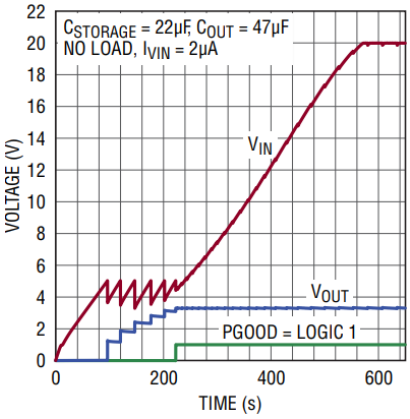

Fig. 8. LTC3588-1 regulator start-up profile [9]

B. Super-capacitors storage and balancing

The circuit used allows two storage configurations, the first possibility is to extend the capacity C_{in} and the second to extend the capacity C_{out}. In both cases, the following relation (Equation 1) defines the exploitable energy:

$$E_{exploitable} = \frac{1}{2} C_{storage} \left({V_{max}}^2 - {V_{min}}^2 \right) \qquad (1)$$

Equation 2 defines the energy ratio (η_{E_ratio}) between the real exploitable energy ($E_{exploitable}$) in the super-capacitors and the theoretically energy available ($E_{th\_available}$) in super-

capacitors. This energy ratio of the super-capacitors makes it possible to do the final solution choice.

$$\eta_{E\_ratio} = \frac{E_{exploitable}}{E_{th\_available}} = \frac{{V_{max}}^2 - {V_{min}}^2}{{V_{\max\_th}}^2} \quad (2)$$

Fig. 9 represents the different topologies that can be used for the storage and the super-capacitors balancing solution.

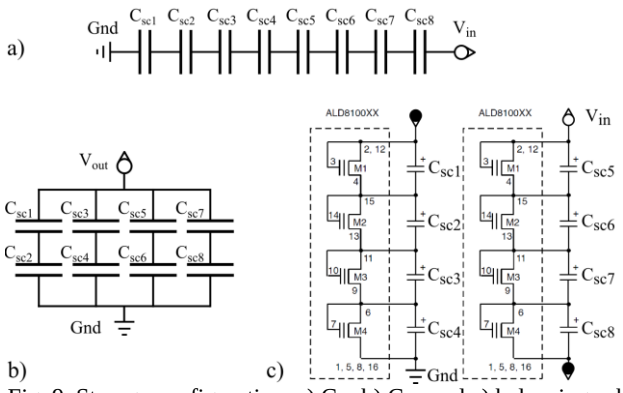

Fig. 9. Storage configuration, a) C_{in}, b) C_{out} and c) balancing sub-system

In the first case (Fig. 9a), it is necessary to use eight super-capacitors of 1 F of 2.7 V in series (V_{max_th} = 21.6 V) in order to obtain a maximum voltage V_{sc} compatible with the extraction circuit of 20 V. This configuration makes it possible to use the buck of the extraction circuit to work on the range of V_{max} = 20 V to V_{min} = 3.67 V and offers an available energy of 24.15 J ($C_{storage}$ = C_{in} = 0.125 F). The energy ratio is 82.8 %. In the second case (Fig. 9b), the maximum voltage is 3.3 V, for the same super-capacitors number, so it is necessary to use four elementary parallel branches each composed of two series super-capacitors of 1 F 2.7 V (V_{max_th} = 5.4 V). This storage block must be followed by a boost to set the required voltage level. For example using a TPS61099 the range of use is V_{max} = 3.3 V to V_{min} = 0.8 V, a usable energy of 10.24 J ($C_{storage}$ = C_{out} = 2 F). The energy ratio is 35.2 % without taking in account the efficiency of the boost, which depends on the current. In this case, the available energy is clearly lower, the super-capacitors are not totally exploited in their integrations and the system is more complex. Therefore, the first storage stage configuration is currently used. But, in the event of a current drain greater than the limit of the circuit capability (100 mA), it is necessary to use a dimensioned capacitance C_{out} [9].

In both cases, the use of several super-capacitors in series requires the use of a balancing system. For this (Fig. 9c), we use an ADLX8100XX component composed of a set of MOSFET transistors acting as variable resistance, thus creating a leakage current reducing the voltage of the capacitors to the desired equilibrium level according to the chip reference used [17].

C. Start energy tuning

The sensor start phase is energy intensive (E_{cold_start} = 389.4 mJ) in comparison with the other phases ($E_{meas.trans.}$ = 3.2 mJ and E_{sleep} = 3.8 mJ). The exploitable energy stored in $C_{storage}$ until the UVLO activates the output is 0.75 J. This energy is sufficient for a sensor start, however if the start phase lasts longer, because the connection is not established properly, the energy is no longer sufficient. To ensure a safety margin, it is possible to delay the activation of the sensor supply by introducing between the extraction circuit and the WSN, a power distribution switch TPS2105 whose activation is performed by a hysteresis low power comparator LTC1540 with adjustable threshold. This solution is represented by the block diagram of Fig. 10a.

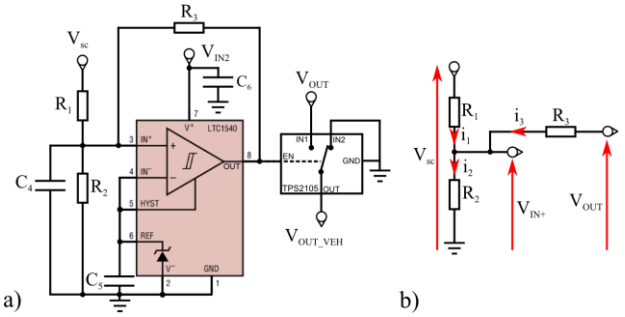

Fig. 10. a) Start energy sub-system block diagram and b) comparator modelling

The LTC1540 compares the image of the super-capacitors voltage (V_{sc}) with respect to an internal reference (V_{ref} = 1.18 V). The comparator is powered by the V_{in2} output of LTC3588-1. When starting the system, this voltage is quickly regulated to 4.8 V. During the start-up phase, this reliable power supply allows the reference voltage (V_{ref}) to be greater than the image of the voltage of V_{sc} and thus to avoid activation of the output at start-up. Capacitors C_4, C_5 and C_6 are filtering capacitors. This comparator has an internal hysteresis of 50 mV too low to be exploited in this application. A feedback loop is then used to increase the hysteresis of the comparator. This comparator is in the high state when the necessary voltage of the super-capacitors V_{sc} is reached (for example V_{sc} = 7 V) and turns off when the low voltage is reached (V_{sc} = 3.67 V same than UVLO falling voltage). Therefore, the energy available is 2.22 J. To size the hysteresis, the comparator can be modelled by Fig. 10b. With this modelling, we can define the values of the resistances necessary for the hysteresis threshold settings. We can write the following relations (equations 3 to 5):

$$i_1 + i_3 = i_2 \quad (3)$$

$$V_{sc} = R_1 i_1 + R_2 i_2 = R_1 i_1 + V_{IN+} \quad (4)$$

$$V_{out} = R_3 i_3 + R_2 i_2 = R_3 i_3 + V_{IN+} \quad (5)$$

From equation 4 and 5, i_1 and i_3 are extracted and injected into equation 3 and the following equation 6 is determined:

$$V_{IN+} = R_2 i_2 = R_2 \left(\frac{V_{sc} - V_{IN+}}{R_1} + \frac{V_{out} - V_{IN+}}{R_3} \right) = \left(\frac{V_{sc}}{R_1} + \frac{V_{out}}{R_3} \right) \frac{R_1 R_2 R_3}{R_1 R_3 + R_2 R_3 + R_1 R_2} \quad (6)$$

Two solutions are possible when $V_{IN+} \approx V_{IN-} \approx V_{ref}$. When V_{IN+} is slightly higher than V_{IN-} then V_{out} = V_{IN2} and V_{sc} = V_{fall}.. When V_{IN+} is slightly lower than V_{IN-} then V_{out} = 0and V_{sc} = V_{rising}. Thanks to the equation 6, then one can

define the thresholds of the hysteresis $V_{fall.}$ and V_{rising} respectively equation 7 and 8.

$$V_{fall.} = \frac{V_{ref}(R_1R_3 + R_2R_3 + R_1R_2)}{R_2R_3} - V_{IN2}\frac{R_1}{R_3} \quad (7)$$

$$V_{rising} = \frac{V_{ref}(R_1R_3 + R_2R_3 + R_1R_2)}{R_2R_3} \quad (8)$$

The difference between $V_{fall.}$ and V_{rising} defines ΔV (equation 9):

$$\Delta V = V_{rising} - V_{fall.} = V_{IN2}\frac{R_1}{R_3} \quad (9)$$

By knowing the desired threshold voltages (V_{rising} and $V_{fall.}$), the supply voltage of the comparator (V_{IN2}) and fixing the resistance R_1 then R_2 and R_3 are deduced naturally from equations 8 and 9. To reduce the current losses in the resistances, the sum of R_1 and R_2 is typically selected to make about 10 MΩ.

5. Experimental powering WSN

A. Vibration energy harvester circuit validation

Different measurement are made on the system. Three measurements are needed to see the different stages of the system's operation: the voltage of the storage; the voltage across the load; the current flowing through it. The characteristic relation of a capacitor (Equation 10) can deduce the charge current of the super-capacitors:

$$i_{sc}(t) = C\frac{dV_{sc}(t)}{dt} \quad (10)$$

A preliminary test was carried out in order to validate the operation and expectations with all the components in order to validate experimentally the circuit represented by Fig. 11:

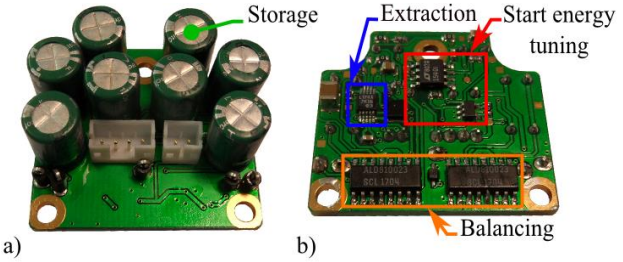

Fig. 11. Experimental circuit (a) front and (b) rear face

To reduce the charging time of the storage stage, due to the weak current of the piezoelectric generator, we use a function generator. It is set to supply a sine wave of 20 V_{pp} at a frequency of 100 Hz and a maximum current of 90 mA. Two resistances loads are used to simulate two types of consumers: 330 Ω and 33 kΩ. The two charges make it possible to highlight the energy balance in the storage and the output consumption. Fig. 12 shows the results of the voltage and current measurements of the storage stage and the terminals of the variable load. At a first start, all the capacitors are empty.

The first phase is the charging phase of the super-capacitors up to the V_{rising} voltage of 7.36 V. The difference with the theoretical V_{rising} voltage of 7 V is due to the quality of the resistances R_1, R_2 and R_3 used to adjust the comparator. Once this voltage is reached the comparator activates the output and the voltage V_{out_VEH} is then 3.28 V. The low load of 330 Ω is connected to the circuit, which result on a dissipated current of 9.9 mA. The voltage level across the super-capacitors decreases slightly to a level of energy balance resulting in a voltage of 7.23 V.

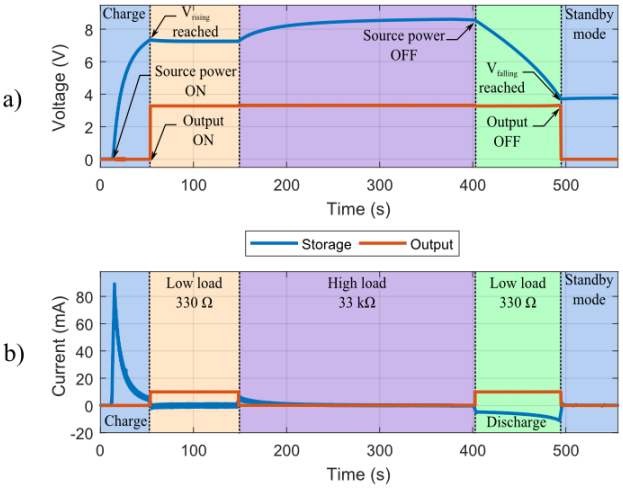

Fig. 12. Validation measurement: a) voltage and b) current

In the next phase, a higher load of 33 kΩ consumes 101 µA. The energy balance allows an increasing of the storage voltage to 8.57 V.

For the next phase, the 330 Ω load is reused to observe the fast discharge of the super-capacitors. When the voltage V_{sc} reaches 3.68 V, the output voltage V_{out_VEH} is zero. This threshold corresponds theoretically to the threshold voltage of the UVLO of the LTC3588-1 circuit as well as the low threshold voltage of the comparator ($V_{UVLO\_falling}$ = $V_{fall.}$). In this case, $V_{fall.}$ is slightly greater than $V_{UVLO\_falling}$. This discharge phase makes it possible to calculate the overall energy efficiency between the energy stored and the energy consumed. The energy stored at the beginning of the phase is 3.74 J. The resistance consumes 3 J in 92.38 s at a power of 32.47 mW (3.28 V x 9.9 mA). The efficiency is then 80.2%. However, according to the data sheet, the yield of LTC3588-1 [9] reduces when the load current is very low (<10 µA). The overall efficiency does not take into account the losses between the power source (function generator or piezoelectric generator) and the storage due to the diode bridge effect, which reduces the voltage by 400 mV and consumes 10 µA.

The last phase shows that the voltage of the super-capacitors remains stable. The majority of components are in sleep mode or the consumption is negligible. This global consumption is about of 751 nA (LTC3588-1: 450 nA, LTC1540: 300 nA and ALD8100XX: <1 nA). The losses related to the theoretical leakage current of the super-capacitors is 10 µA. This partial load allows a faster system restart.

B. *WSN powered by VEH*

The Fig. 13 shows the piezoelectric generator employed with the performance presented previously and the integrated electronic.

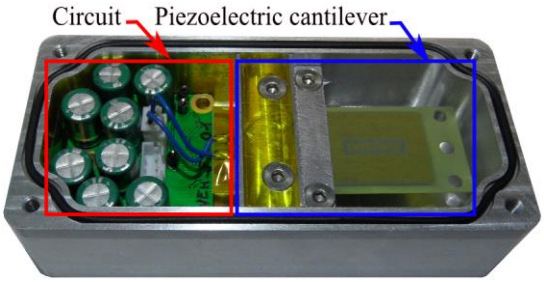

Fig. 13. Piezoelectric vibration energy harvester

Fig. 14 represents the time evolution of the VEH storage stage voltage (V_{sc}) and output voltage (V_{out_VEH}) to supply the JENNIC JN5148 WSN.

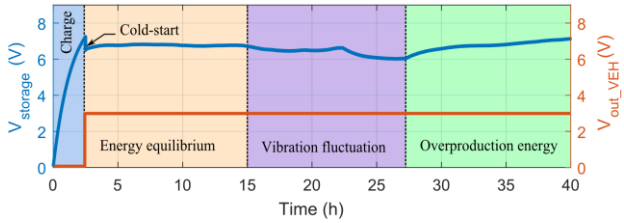

Fig. 14. Storage voltage and output evolution

Several events are observable on this statement. The first phase is the super-capacitors load up to 7.23 V. The start threshold being reached the power distribution switch is activated (V_{out_VEH} goes to 3.28V) and then the WSN enters its phase of initialisation which empties partially the super-capacitors. Quickly, the WSN alternates between the sleep phase and the measurement and transmission phase. The fact that the super-capacitors voltage seems to stabilize shows that there is an equilibrium between the energy produced and the energy consumed. Then, it appears an important phase of discharge to be linked to fluctuations of the vibration source (frequency or acceleration variations). The last phase shows an over-production of energy by the piezoelectric generator. During more than 33 h, the WSN keeps its connection with the coordinator while transmitting measurements every 48 seconds.

6. Conclusion

This paper presents an electronic architecture for the management of electrical energy. This energy is extracted from a vibratory energy harvester to power a JENNIC JN5148 WSN. This structure uses few components, all commercially available, with simple functionality while maximizing the energy stored during energy intensive phases. Circuit validation tests show performance and expected behaviour. The low consumption of the elements used makes it possible to obtain a yield between the stored energy and the usable energy greater than 80%. The long duration test shows a good functioning of the architecture used and makes it possible to reduce the impact of vibration source availability or WSN connection to its hub.

Acknowledgement

This work was supported by the 2IDO project (Internet Industriel des Objets et des Opérateurs in french) on the wireless sensor node development. The authors gratefully acknowledge this support.

References

[1] Libelium, "www.libelium.com," *Libelium Smart World*.

[2] S. Kim *et al.*, "Health monitoring of civil infrastructures using wireless sensor networks," in *2007 6th International Symposium on Information Processing in Sensor Networks*, 2007, pp. 254–263.

[3] A. Mainwaring, D. Culler, J. Polastre, R. Szewczyk, and J. Anderson, "Wireless sensor networks for habitat monitoring," in *International Workshop on Wireless Sensor Networks and Applications*, 2002, pp. 88–97.

[4] G. Werner-Allen *et al.*, "Deploying a wireless sensor network on an active volcano," *IEEE Internet Comput.*, vol. 10, pp. 18–25, 2006.

[5] J. Gubbi et al., "Internet of Things (IoT): A vision, architectural elements, and future directions," *Futur. Gener. Comput. Syst.*, vol. 29, no. 7, pp. 1645–1660, 2013.

[6] Ovum, "www.ovum.informa.com," *Ovum IoT Entrep. Insight Surv.*

[7] S. Priya and D. J. Inman, *Energy harvesting technologies*. 2008.

[8] S. Priya *et al.*, "A Review on Piezoelectric Energy Harvesting: Materials, Methods, and Circuits," *Energy Harvest. Syst.*, vol. 4, no. 1, 2017.

[9] Linear Technology, "www.analog.com," *LTC3588-1*.

[10] L. Chen, X. Xu, P. Zeng, and J. Ma, "Integration of energy harvester for self-powered wireless sensor network nodes," *Int. J. Distrib. Sens. Networks*, vol. 2014, no. April, 2014.

[11] X. Zhang, J. Fang, F. Meng, and X. Wei, "A novel self-powered wireless sensor node based on energy harvesting for mechanical vibration monitoring," *Math. Probl. Eng.*, vol. 2014, 2014.

[12] Y. Jiang, S. Shiono, and H. Hamada, "Low-frequency energy harvesting using a laminated PVDF cantilever with a magnetic mass," in *PowerMEMS 2010*, 2010, p. 375.

[13] A. M. Stamatellou and A. I. Kalfas, "Experimental investigation of energy harvesting from swirling flows using a piezoelectric film transducer," *Energy Convers. Manag.*, vol. 171, no. May, pp. 1405–1415, 2018.

[14] MIDE, "www.mide.com," *MIDE PPA1014*.

[15] F. Huet and V. Boitier, "Banc de caractérisation de récupérateurs d'énergie vibratoire : Application sur dispositif piézoélectrique pour l'alimentation de capteurs communicants sans fil.," in *CETSIS 2018*, 2018.

[16] A. Badel, "Récupération d'énergie et contrôle vibratoire par éléments piézoélectriques suivant une approche non linéaire."

[17] R. L. Chao, "MOSFET-based current balancing cuts power use in supercapacitors stacks," *Adv. Linear Devices Inc.*, 2015.